

- 1     **UCT943, a next generation *Plasmodium falciparum* PI4K inhibitor preclinical**  
2     **candidate for the treatment of malaria**  
3  
4     Christel Brunschwig<sup>a</sup>, Nina Lawrence<sup>a</sup>, Dale Taylor<sup>a</sup>, Efrem Abay<sup>a</sup>, Mathew Njoroge<sup>a</sup>, Gregory  
5     S. Basarab<sup>a</sup>, Claire Le Manach<sup>b</sup>, Tanya Paquet<sup>b</sup>, Diego González Cabrera<sup>b</sup>, Aloysius T.  
6     Nchinda<sup>b</sup>, Carmen de Kock<sup>a</sup>, Lubbe Wiesner<sup>c</sup>, Paolo Denti<sup>c</sup>, David Waterson<sup>d</sup>, Benjamin  
7     Blasco<sup>d</sup>, Didier Leroy<sup>d</sup>, Michael J. Witty<sup>d</sup>, Cristina Donini<sup>d</sup>, James Duffy<sup>d</sup>, Sergio Wittlin<sup>e,f</sup>,  
8     Karen L. White<sup>g</sup>, Susan A. Charman<sup>g</sup>, Maria Belén Jiménez-Díaz<sup>h</sup>, Iñigo Angulo-Barturen<sup>h</sup>,  
9     Esperanza Herreros<sup>h</sup>, Francisco Javier Gamo<sup>h</sup>, Rosemary Rochford<sup>i</sup>, Dalu Mancama<sup>j</sup>, Theresa  
10    L. Coetzer<sup>k</sup>, Mariëtte E. van der Watt<sup>l</sup>, Janette Reader<sup>l</sup>, Lyn-Marie Birkholtz<sup>l</sup>, Kennan C.  
11    Marsh<sup>m</sup>, Suresh M. Solapure<sup>n</sup>, Manu Vanaerschot<sup>o</sup>, David A. Fidock<sup>o,p</sup>, Paul V. Fish<sup>q</sup>, Peter  
12    Siegl<sup>r</sup>, Dennis A. Smith<sup>s</sup>, Grennady Wirjanata<sup>t</sup>, Rintis Noviyanti<sup>u</sup>, Ric N. Price<sup>t,v</sup>, Jutta Marfurt<sup>t</sup>,  
13    Kigbafori D. Silue<sup>w</sup>, Leslie J. Street<sup>b</sup>, Kelly Chibale<sup>b,x,y #</sup>  
14  
15    <sup>a</sup> Drug Discovery and Development Centre (H3D), Division of Clinical Pharmacology,  
16    Department of Medicine, University of Cape Town, Observatory, 7925, South Africa  
17    <sup>b</sup> Drug Discovery and Development Centre (H3D), Department of Chemistry, University of  
18    Cape Town, Rondebosch 7701, South Africa  
19    <sup>c</sup> Division of Clinical Pharmacology, Department of Medicine, University of Cape Town,  
20    Observatory, 7925, South Africa  
21    <sup>d</sup> Medicines for Malaria Venture, ICC, Route de Pré -Bois 20, P.O. Box 1826, 1215 Geneva,  
22    Switzerland  
23    <sup>e</sup> Swiss Tropical and Public Health Institute, Socinstrasse 57, 4002 Basel, Switzerland

- 24 <sup>f</sup> University of Basel, 4003 Basel, Switzerland
- 25 <sup>g</sup> Centre for Drug Candidate Optimisation, Monash University, 381 Royal Parade, Parkville,  
26 Melbourne, Victoria 3052 Australia
- 27 <sup>h</sup> GlaxoSmithKline, Tres Cantos Medicines Development Campus, Severo Ochoa, 2, 28760  
28 Tres Cantos, Madrid, Spain
- 29 <sup>i</sup> Departments of Immunology and Microbiology, University of Colorado, Denver, Aurora,  
30 CO, United States
- 31 <sup>j</sup> Biosciences, Council for Scientific and Industrial Research, PO Box 395, Pretoria 0001, South  
32 Africa
- 33 <sup>k</sup> Plasmodium Molecular Research Unit, Wits Research Institute for Malaria, Department of  
34 Molecular Medicine and Haematology, School of Pathology, Faculty of Health Sciences,  
35 University of the Witwatersrand and National Health Laboratory Service, Johannesburg  
36 2193, South Africa
- 37 <sup>l</sup> Department of Biochemistry, Institute for Sustainable Malaria Control and South African  
38 Medical Research Council Collaborating Centre for Malaria Research, University of Pretoria,  
39 Private Bag x20, Hatfield, Pretoria 0028, South Africa
- 40 <sup>m</sup> AbbVie, 1 North Waukegan Road, North Chicago, IL 60064-6104, United States
- 41 <sup>n</sup> Nagarjuna Gardens, 60 Feet Road, Sahakaranagar, Bangalore 560092, India
- 42 <sup>o</sup> Department of Microbiology and Immunology, Columbia University Medical Center, New  
43 York, New York 10032, United States
- 44 <sup>p</sup> Division of Infectious Diseases, Department of Medicine, Columbia University Medical  
45 Center, New York, New York 10032, United States

<sup>q</sup> Alzheimer's Research UK UCL Drug Discovery Institute, Faculty of Brain Sciences, University  
College London, Gower Street, London, United Kingdom  
<sup>r</sup> Siegl Pharma Consulting LLC, Blue Bell, PA, United States  
<sup>s</sup> 4 the Maltings, Walmer, Kent, United Kingdom  
<sup>t</sup> Global and Tropical Health Division, Menzies School of Health Research, Charles Darwin  
University, PO Box 41096, Casuarina, NT 0811, Darwin, Australia  
<sup>u</sup> Eijkman Institute for Molecular Biology, Jalan Diponegoro 69, 10430 Jakarta, Indonesia  
<sup>v</sup> Centre for Tropical Medicine and Global Health, Nuffield Department of Clinical Medicine,  
University of Oxford, United Kingdom  
<sup>w</sup> Centre Suisse de Recherches Scientifiques en Côte d'Ivoire, Km17 Route de Dabou,  
Adipodoumé, 01 BP 1303 Abidjan, Côte d'Ivoire  
<sup>x</sup> Institute of Infectious Disease and Molecular Medicine, University of Cape Town,  
Rondebosch 7701, South Africa  
<sup>y</sup> South African Medical Research Council Drug Discovery and Development Research Unit,  
Department of Chemistry, University of Cape Town, Rondebosch 7701, South Africa  
#corresponding author: [kelly.chibale@uct.ac.za](mailto:kelly.chibale@uct.ac.za)

62

## 63 Abstract

64 The 2-aminopyridine MMV048 was the first drug candidate inhibiting *Plasmodium*  
65 phosphatidylinositol 4-kinase (PI4K), a novel drug target for malaria, to enter clinical  
66 development. In an effort to identify the next generation of PI4K inhibitors, the series was  
67 optimized to improve properties such as solubility and antiplasmodial potency across the  
68 parasite lifecycle, leading to the 2-aminopyrazine UCT943. The compound displayed higher

69 asexual blood stage, transmission-blocking, and liver stage activity than MMV048 and was  
70 more potent against resistant *P. falciparum* and *P. vivax* clinical isolates. Excellent *in vitro*  
71 antiparasmodial activity translated into high efficacy in *P. berghei* and humanized *P.*  
72 *falciparum* NOD-*scid* IL-2R $\gamma^{null}$  mouse models. The high passive permeability and high  
73 aqueous solubility of UCT943, combined with low to moderate *in vitro* intrinsic clearance,  
74 resulted in sustained exposure and high bioavailability in preclinical species. In addition, the  
75 predicted human dose for a curative single administration using monkey and dog  
76 pharmacokinetics was low, ranging from 50 to 80 mg. As a next generation *Plasmodium* PI4K  
77 inhibitor, the combined preclinical data suggest that UCT943 has the potential to form part  
78 of a single-exposure radical cure and prophylaxis (SERCaP) to treat, prevent and block the  
79 transmission of malaria.

80

## 81 1 INTRODUCTION

82 Malaria, an infectious disease transmitted to people through the bite of female *Anopheles*  
83 mosquitoes infected with *Plasmodium falciparum* (Pf) or *Plasmodium vivax* (Pv), still afflicts  
84 millions of people, with almost 90% of cases on the African continent. Even though the  
85 number of malaria cases has fallen globally from an estimated 237 million cases in 2010 to  
86 216 million cases in 2016, malaria still causes 445 000 deaths per year, 99% of which are due  
87 to Pf in Africa (1). Parasite resistance against currently recommended artemisinin-based  
88 combination therapies (2, 3) is a concern, and antimalarial drugs with a novel mode of  
89 action are urgently needed. We previously reported the identification of the 2-  
90 aminopyridine compound MMV390048 (also known as MMV048), which is efficacious *in*  
91 *vivo* against all measurable *Plasmodium* life cycle stages, except hypnozoites (4). MMV048

92 acts through the inhibition of *Plasmodium* phosphatidylinositol 4-kinase (PI4K) and is the  
93 first and sole agent with this mode of action that has entered clinical development. PI4K was  
94 reported as a target for *Plasmodium* in 2013 with inhibition by other compound classes (5).  
95 The low aqueous solubility associated with MMV048 in biorelevant media was identified as  
96 one of the issues to address in the next generation of PI4K inhibitors along with improved  
97 potency. Towards this goal, a scaffold change from the 2-aminopyridine to the 2-  
98 aminopyrazine core with concomitant introduction of aqueous solubilizing groups delivered  
99 analogues with a better developability profile with respect to improved physicochemical  
100 properties, as well as a significant improvement in potency across the parasite lifecycle .  
101 Improved aqueous solubility was optimally achieved through the incorporation of a  
102 piperazinylamide group on the phenyl ring at the 5-position of the 2-aminopyrazine scaffold,  
103 leading to UCT943 (Figure 1). This compound, among other attributes, showed potent *in*  
104 *vitro* activity against multiple stages of the parasite lifecycle and excellent *in vivo* efficacy in  
105 the *Plasmodium berghei* and *P. falciparum* NSG (NOD-*scid* IL-2R $\gamma^{null}$ ) mouse models (6). In  
106 order to assess the potential of UCT943 as a follow-on compound to MMV048 and a  
107 preclinical antimalarial candidate, physicochemical, parasitological, and pharmacological  
108 profiling was undertaken. Furthermore, extensive drug metabolism and pharmacokinetics  
109 (DMPK) profiling was carried out in order to facilitate the prediction of human  
110 pharmacokinetic (PK) parameters and the efficacious single dose in humans. The results are  
111 reported herein.

## 112 2 MATERIAL AND METHODS

113 2.1 Chemistry

114 UCT943 was synthesized in seven steps from commercially available 2-aminopyrazine, as  
115 previously described (6).

116 2.2 *In vitro* antiparasmodial activity

117 2.2.1 *Asexual blood stage assays*

118 2.2.1.1 *Cross-resistance against field isolates*

119 UCT943 was tested using the [<sup>3</sup>H]-hypoxanthine incorporation assay (7, 8) against a panel of  
120 drug sensitive and drug resistant *P. falciparum* strains (Supplementary Material Table S1), as  
121 well as against a panel of resistant *P. falciparum* clones generated in the laboratory of Prof  
122 David Fidock (Columbia University, USA) (Supplementary Material Table S2).

123 2.2.1.2 *In vitro P. falciparum resistance generation to UCT943 and pi4k gene sequencing*

124 The generation of UCT943-resistant *Pf* clones was performed as described elsewhere (4)  
125 (see Supplementary Material Table S4).

126 2.2.1.3 *Ex vivo assay against resistant P. falciparum clinical isolates from Côte d'Ivoire*

127 Drug susceptibility of *P. falciparum* isolates from Côte d'Ivoire, West Africa was measured  
128 using incorporation of SYBR® Green into the parasite's DNA as described before (9). The  
129 drug plates contained 10 serial concentrations of the antimalarials, with maximum  
130 concentration of 1170 nM for UCT943.

131 2.2.1.4 *Ex Vivo schizont maturation drug susceptibility assay against P. vivax and P.*

132 *falciparum clinical isolates*

133 Drug susceptibility of *P. vivax* and *P. falciparum* isolates from Papua, Indonesia was  
134 measured using a modified schizont maturation assay as described previously (9). The drug  
135 plates contained 11 serial concentrations of the antimalarials, with maximum

136 concentrations of 2993 nM for chloroquine, 1029 nM for piperaquine, 338 nM for  
137 mefloquine, 49 nM for artesunate, and 297 nM for UCT943.

138 *2.2.2 Liver stage assays*

139 *2.2.2.1 P. berghei liver stage assay*

140 *Plasmodium berghei* luciferase sporozoites were obtained by dissection of infected  
141 *Anopheles stephensi* mosquito salivary glands. The sporozoite invasion assay was performed  
142 as described in (6) using the rodent parasite *P. berghei* that is able to infect human  
143 hepatocarcinoma HepG2-A16-CD81EGFP cells (10, 11).

144 *2.2.2.2 P. cynomolgi liver stage assay*

145 Primary rhesus hepatocytes were infected *in vitro* with *P. cynomolgi* sporozoites and the  
146 drug assays performed as previously reported by Zeeman *et al.* (12).

147 *2.2.2.3 P. vivax liver stage assay*

148 The *P. vivax* liver stage assay was implemented in human hepatocytes, infected *in vitro* with  
149 *P. vivax* sporozoites, according to the protocol described in (13).

150 *2.2.3 Gametocyte assays*

151 *In vitro* gametocytocidal activity was determined using luciferase reporter lines specifically  
152 enabling screening against early stage gametocytes (>90% stage I-III) and late stage  
153 gametocytes (>95% stage IV-V) as per Reader *et al.* (14). Methylene blue (5  $\mu$ M) and  
154 MMV048 (5  $\mu$ M) were routinely included as controls.

155 *2.2.4 P. falciparum Dual Gamete Formation Assay (Pf DGFA)*

156 Transmission-blocking activity of UCT943 was assessed in the DGFA, which utilizes a dual  
157 read-out that individually and simultaneously reports on the functional viability of male and  
158 female mature stage V gametocytes, as per Ruecker *et al.* (15).

## 159 2.3 Physicochemical properties

160 The pKa of UCT943 was determined by potentiometric titration as described previously (16).  
161 Solubility was measured after 24 h incubation of solid material with media at 37°C with  
162 residual solids checked by XRPD. Media included five pH buffers (pH 2.0, 4.0, 6.0, 8.0, and  
163 10.0) and three bio-relevant media: Simulated Gastric Fluid (SGF) pH 1.8, Fasted State  
164 Simulated Intestinal Fluid (FaSSIF) pH 6.5 and Fed State Simulated Intestinal Fluid (FeSSIF)  
165 pH 5.0. Analyses were done by High Performance Liquid Chromatography (HPLC) (Waters  
166 Xbridge C18, 150 × 4.6 mm, 3 µm) at 40°C with a mobile phase of 0.1% trifluoroacetic acid  
167 (TFA) in water and 0.1% TFA in acetonitrile with UV detection (220 nm, reference 500 nm).

168 2.4 *In vitro* metabolism studies

169 Metabolic stability of UCT943 (1 µM) was assessed in human, dog, rat, and mouse liver  
170 microsomes using a 5-point assay and LC-MS/MS as described in (17). Metabolic stability (1  
171 µM) was also evaluated with cryopreserved hepatocytes from the same species (1 × 10<sup>6</sup>  
172 viable cells/mL), as described in (18). Hepatic extraction ratio's (E<sub>H</sub>) were calculated using  
173 physiological based scaling factors as previously described (19).

174 Binding to plasma proteins and microsomal proteins (0.5 mg/mL) was determined by  
175 ultracentrifugation with LC-MS analysis as described in (20) and (17), respectively.

176 Permeability was determined across Caco-2 monolayers in both apical to basolateral and  
177 basolateral to apical directions using pH 7.4 in both apical and basolateral chambers, as  
178 reported in (9).

179 Cytochrome P450 (CYP450) inhibition studies (CYP2D6, CYP2C9, CYP3A4/5) were carried out  
180 with pooled human liver microsomes using the conditions described in (21). Metabolite  
181 identification was performed by LC-MS/MS, as described in (22), with a Phenomenex



182 Kinetex PFP column, 2.1 mm x 100 mm, 2.6  $\mu$ m particles using microsomal incubations,  
183 incubations in hepatocytes from the hepatocyte stability assay, and *in vivo* mouse PK  
184 samples.  
185 Plasma stability and whole blood-to-plasma partitioning ratio (B:P) were determined by  
186 spiking blood from humans (Australian Red Cross Blood bank), dogs, rats, or mice with  
187 UCT943 and incubating for 4 h at 37°C. During the incubation period, aliquots of blood were  
188 taken to confirm stability. At the end of the incubation period, duplicate aliquots of blood  
189 were taken and the remaining sample was centrifuged to collect duplicate aliquots of  
190 plasma. Concentrations in blood and the plasma fraction of blood were measured by LC-MS  
191 and the blood to plasma concentration ratio calculated using the mean concentration for  
192 each matrix.

## 193 2.5 Ethics statement

194 Animal experiments were approved by the institutional animal care and use committees for  
195 each of the experimental sites. All studies were conducted according to the appropriate  
196 legislation and respective institutional policies on animal use and welfare.  
197 The human biological samples were sourced ethically and their research use was in accord  
198 with the terms of the informed consents.

## 199 2.6 Pharmacokinetic studies

200 Pharmacokinetic studies were performed in mice, rats, dogs and monkeys as described in  
201 the Supplementary Material. For comparison of blood clearance ( $CL_b$ ) to hepatic blood flow,  
202 values of 90, 55, 31, 44, and 21 mL/min/kg were assumed in mice, rats, dogs, monkeys, and  
203 humans, respectively (23).

204 2.7 *In vivo* efficacy studies

205 *In vivo* efficacy studies were conducted in the *P. berghei* and in the *P. falciparum* NOD-*scid*

206 *IL-2R $\gamma$ <sup>null</sup>* (NSG) model as described previously (6, 24) (see Supplementary Material).

207 2.8 Prediction of human pharmacokinetics and efficacious single dose by

208 pharmacokinetic/pharmacodynamic (PK/PD) modeling

209 2.8.1 Allometric scaling

210 The calculation of human plasma clearance (CL<sub>p</sub>) and human plasma volume of distribution

211 at steady state (V<sub>ss</sub>) for UCT943 was carried out by a hybrid approach to allometric inter-

212 species scaling (mouse, rat, dog, and monkey) of *in vivo* plasma CL<sub>p</sub> and V<sub>ss</sub> (25). After

213 logarithmic/logarithmic transformation, the parameters were fitted to the equation  $\log y =$

214  $\log a + b \log BW$ , where BW is body weight; a and b are the allometric coefficient and

215 exponent, respectively. Body weights of 0.025; 0.3; 5; 10 and 70 kg were used for mice, rats,

216 monkeys, dogs, and humans, respectively. The mean residence time (MRT) was calculated

217 from the predicted human plasma V<sub>ss</sub> divided by the predicted human plasma CL<sub>p</sub>.

218 2.8.2 PK/PD analysis in the *Pf*-infected NSG mouse model to predict minimum parasitocidal

219 concentration (MPC)

220 Blood PK data from *Pf*-infected NSG mice were first fitted to a one-compartment model with

221 first-order absorption and elimination. The predicted PK profiles were used to run a direct

222 effect (DE) PK/PD model using Phoenix WinNonlin® (Certara, Princeton, NJ) in order to

223 determine the minimum parasitocidal concentration (MPC) of UCT943 (Supplementary

224 Material Equation S1 and S2).

225 2.8.3 *Simulation of human PK profiles for human dose prediction*

226 Dog and monkey data were used to predict human PK, since higher species allow more  
227 extensive blood sampling to explore blood or plasma concentration against time curves in  
228 detail. Intravenous (IV) and oral (PO) time course profiles were normalized in PKSolver  
229 (Excel) for preclinical species and Wajima-transformed (26). The absorption rate constant  
230 ( $k_a$ ), and the bioavailability (F) estimates were obtained from PKSolver using the Wajima-  
231 transformed data. Human PO PK parameters were predicted in Berkeley Madonna  
232 (University of California, Berkeley, CA) using the Wajima transformed PK data, the human PK  
233 parameters obtained from allometry in section 2.8.1, and the  $K_a$  and F estimates, to have  
234 drug concentration above the MPC for  $\geq 8$  days. The single dose required to maintain the  
235 human plasma concentration above the MPC for eight days (section 2.8.2) was determined  
236 through simulation using the human PO PK profiles with Berkeley Madonna.

237 2.9 *In vitro* cytotoxicity, cardiotoxicity and genotoxicity

238 2.9.1 *Cytotoxicity*

239 *In vitro* cytotoxicity of UCT943 was tested against L6 cells using the Alamar Blue assay, and  
240 against Chinese Hamster Ovarian (CHO), Vero, and HepG2 cells, using the 3-(4,5-  
241 dimethylthiazol-2-yl)-2,5-diphenyltetrazoliumbromide (MTT) assay (27, 28).

242 2.9.2 *Cardiotoxicity*

243 UCT943 was tested for inhibition of the human ether a go-go related gene (hERG)  $K^+$  channel  
244 ( $K_v11.1$ ), human  $K_v1.5$   $K^+$  channel, and human voltage-gated sodium channel  $Na_v1.5$  using  
245 IonWorks patch clamp electrophysiology (29), and for inhibition of the human  $Ca_v1.2$   
246 calcium channel (cardiac L-type) using a fluorescence  $Ca^{2+}$  assay. For all assays, 50%

247 cytotoxic concentrations ( $CC_{50}$ ) were determined from 8-point dose-response curves

248 generated using 3-fold serial dilutions from the maximum final assay concentration.

### 249 2.9.3 Genotoxicity

#### 250 2.9.3.1 Ames

251 UCT943 was assessed for mutagenic toxicity by measuring its ability to induce reverse

252 mutations in the *Salmonella typhimurium*-*Escherichia coli*/microsome plate incorporation

253 assay (30, 31). Maximum concentrations were 5000  $\mu$ g per plate.

#### 254 2.9.3.2 Micronucleus

255 UCT943 capability to induce clastogenicity/aneugenicity in CHO-WBL cells was determined

256 by measuring the extent of micronucleus formation with and without exogenous metabolic

257 activation (Aroclor 1254 induced rat liver S9). Maximum concentrations were 500  $\mu$ g/mL.

### 258 2.10 *In vivo* glucose-6-phosphate dehydrogenase (G6PD)-hemolysis

259 *In vivo* hemolytic toxicity was assessed in NOD-scid mice engrafted with A- G6PD-deficient

260 human red blood cells (huRBCs) as described in (32) following 4-day treatment regimen at

261 1.5 and 10 mg/kg/day dose levels given orally.

## 262 3 RESULTS AND DISCUSSION

### 263 3.1 Rationale for optimization of MMV048 resulting in UCT943

264 Although MMV048 showed good potency against asexual blood stage parasites, there was

265 room for improvement with respect to activity against liver and the transmissible

266 gametocyte stage parasites(4).

267 During First-In-Human (FIH) studies, MMV048 showed high variability in exposure, which

268 was attributed to low solubility. Intensive and time consuming formulation work had to be

269 carried out in order to identify a new formulation with a more consistent and 3-fold greater  
270 exposure ([www.mmv.org/newsroom/interviews/mmv048-0](http://www.mmv.org/newsroom/interviews/mmv048-0)).  
271 To avoid such developability issues in future, improved solubility, pH-dependent and in  
272 biorelevant media, was identified as the main differentiating factor in follow-on compounds.  
273 Thus chemical modifications to MMV048 were made in such a way as to incorporate  
274 solubility-enhancing moieties. In this regard, the methyl sulfonyl group of MMV048 was  
275 replaced by a water solubilizing piperazinyl carboxamide on the phenyl ring at the 5-position  
276 of the 2-aminopyrazine core to deliver UCT943 (6). Improvements in asexual blood stage  
277 and liver stage activities were achieved by replacing the 2-aminopyridine ring with a 2-  
278 aminopyrazine ring, which also maintained good potency against gametocytes (6). One key  
279 objective of this study was firstly to determine if these improvements would translate into  
280 better in vivo efficacy in the *Pf*-infected NSG mouse model and accordingly, a low  
281 predicated human dose.

### 282 3.2 *In vitro* antiplasmodial activity

283 The biological target of the clinical candidate MMV048 was identified to be *Plasmodium*  
284 phosphatidylinositol 4-kinase (PI4K) through resistant mutant generation, sequencing, and  
285 pull-down experiments (4). *Plasmodium* PI4K has recently been identified as a new and  
286 promising drug target, which is present at all life-cycle stages of the *Pf* and *Pv* parasites (5).  
287 UCT943 inhibits the *Pv*PI4K enzyme with an  $IC_{50} = 23$  nM. When tested against a 5-fold  
288 resistant *P. falciparum* strain generated against MMV048 due to the mutated *pfpi4k* locus  
289 (4), UCT943 displayed a 6-fold shift in  $IC_{50}$  relative to the parental Dd2 strain (14 nM relative  
290 to 2.2 nM) (Supplementary Material Table S2). When resistance was selected for in Dd2-B2  
291 using UCT943, *pfpi4k* mutants with a 4- or 8-fold  $IC_{50}$  shift were obtained (Supplementary

Material Table S3). These mutants carried the G1309V or Y1342F mutations respectively, and are located in the same region of *pi4k* as MMV048-selected mutations reported elsewhere (4). Resistance selection studies indicated a minimum required inoculum of  $10^7$  Dd2 parasites for resistance to emerge, which is similar to MMV048 (4). By comparison,  $IC_{50}$  shifts were within 2-fold when tested against strains containing mutated loci in either *pfcytB*, *pf dhodh*, *pfatp4*, or *pfcarl*. These data indicate that UCT943 and MMV048 have the same molecular target, and that similarly to MMV048, UCT943 is expected to have transmission blocking and liver stage activity. Importantly, UCT943 maintained high *in vitro* selectivity (> 200 fold) for the parasite PvPI4K versus the human PI4KB isozyme ( $IC_{50}$  (PI4KB) = 5.4  $\mu$ M), which inhibition is linked to immunosuppressive effects (33).

UCT943 was one of the most potent compounds assessed in the 2-aminopyrazine chemical series (6), with  $IC_{50}$ 's of 5.4 and 4.7 nM against NF54 and K1 *P. falciparum* strains, respectively, which was 5- to 6-fold more active than the clinical candidate MMV048 (4) (Figure 2). In addition, UCT943 was equally active against the drug sensitive NF54 strain and multi-drug resistant strains, with  $IC_{50}$ 's ranging from 4 to 7 nM, thus suggesting that cross-resistance with existing antimalarials is a low risk (Supplementary Material Table S1).

UCT943 primarily exhibited blood stage activity against schizonts (Supplementary Material Table S5), which correlates with a slow rate of kill as determined in the *in vitro* parasite reduction ratio (PRR) assay (lag phase = 48 h, Log PRR = 2.5 at 10 x  $EC_{50}$  in 3D7 strain) and in the *in vitro* speed assay (Supplementary Material Table S5). As expected, the killing rate profile of UCT943 was similar to that of MMV048 (lag phase = 48 h, Log PRR = 2.7) (4). When tested against *Pf* clinical isolates of the Ivory Coast, UCT943 exhibited potent activity (2-15 nM) (Supplementary Material Table S6). The potency of UCT943 against clinical isolates

315 from Papua Indonesia was significantly higher than that of MMV048 in *Pv* and in *Pf* (median  
316  $IC_{50}$  14 nM and 29 nM;  $p=0.012$  versus median  $IC_{50}$  93 nM and 202 nM;  $p<0.001$ ) (Figure 2  
317 and Supplementary Material Table S7). Interestingly, both compounds displayed higher  
318 potency against *Pv* than *Pf*, a trend that was also observed for another PI4K inhibitor,  
319 KDU691, albeit to a lesser extent (5).

320 When tested against other stages of the parasite life cycle (Figure 2), UCT943 was 2-50  
321 times more potent than MMV048 (4). UCT943 was potent against early stage (>90% stage I-  
322 III) and late stage gametocytes (>95% stage IV-V) ( $IC_{50}$  of 134 nM and 66 nM, respectively)  
323 and inhibited the formation of both male and female gametes ( $IC_{50} \approx 80$  nM) in the dual  
324 gamete formation assay (DGFA). The latter activity translated into transmission-blocking  
325 activity (Target Candidate Profile TCP5 as defined by Burrows *et al.* (34)) in the standard  
326 membrane feeding assay (SMFA), with an  $IC_{50}$  of 96 nM (35), equivalent to MMV048 (Figure  
327 2). In-depth clinical PK/PD investigations would be needed to determine doses that would  
328 afford coverage for both blood stage and transmission-blocking activities. A single drug with  
329 both activities would be a valuable addition to the arsenal of antimalarial medicines.

330 UCT943 also exhibits better *in vitro* liver stage activity than MMV048 (potentially addressing  
331 TCP3 and TCP4 (34)), targeting schizonts *in vitro* ( $IC_{50}$  of < 100 nM and <10 nM in *P. vivax*  
332 and *P. cynomolgi*, respectively, when tested prophylactically, and 0.92 nM in *P. berghei*), as  
333 well as inhibiting the formation of hypnozoites ( $IC_{50}$  of < 100 nM and < 10 nM in *P. vivax* and  
334 *P. cynomolgi*, respectively when tested prophylactically) (Figure 2). The parasitophorous  
335 vacuole membrane protein UIS4 becomes internalized in MMV048-treated *P. berghei*  
336 HepG2 cultures, a morphology associated with *in vitro* liver stage parasite clearance(4).

337 Though UCT943 was not evaluated for such morphological changes, its activity against  
338 schizonts offers prospects for improved prophylactic liver stage activity relative to MMV048.

### 339 3.3 Physicochemical characterization

340 UCT943 was stable in the solid state over a period of 18 months and was chemically stable  
341 at 20°C in solutions of DMSO, water (pH 6.2), and buffers (pH 2, pH 7.4) over 6 days.

342 The piperazinylamide group accounts for the significantly lower measured lipophilicity of  
343 UCT943 (LogD = -0.27) relative to MMV048 (LogD = 2.6). This, combined with a pKa of 7.5,  
344 results in higher measured solubility in aqueous media compared to MMV048, across a  
345 range of physiologically relevant pH's up to 6.5, where the compound is protonated (Table  
346 1). The compound was also highly soluble in SGF (pH 1.8), FeSSIF (pH 5.0), and FaSSIF media  
347 (pH 6.5) (> 1.5 mg/mL), predictive of a good dissolution in the gastrointestinal tract. The pH-  
348 dependent solubility profile of UCT943 in aqueous media was typical of a weak base with  
349 higher solubility at pH below the pKa, *i.e.* 7.5 (Figure 3). UCT943 exhibited high permeability  
350 across Caco-2 cells in both directions ( $P_{app\ B\rightarrow A} = 25 \times 10^{-6}$  cm/s;  $P_{app\ A\rightarrow B} = 28 \times 10^{-6}$  cm/s)  
351 without appreciable efflux (efflux ratio of 0.93, Table 2). With high FaSSIF solubility and high  
352 permeability, UCT943 could be classified as a Developability Classification System (DCS)  
353 Class I compound, which bodes well for a much more favorable development pathway  
354 compared to MMV048 that was classified as DCS Class II (Figure 4) (36). The high solubility  
355 and permeability of UCT943, along with its potent anti-*Plasmodium* activity against all  
356 stages of the parasite lifecycle (see section 3.1) triggered comprehensive DMPK profiling  
357 toward determining its potential for preclinical development.



358 3.4 *In vitro* and *in vivo* metabolism studies

359 There was no evidence of chemical instability for UCT943 in human, dog, rat, or mouse  
360 blood or plasma. The compound was moderately bound to plasma proteins with little  
361 species differentiation ( $f_u$  in plasma 0.10-0.16). It also had a greater propensity than  
362 MMV048 (B:P ~1.0 across species) to bind or distribute in red blood cells (RBCs) relative to  
363 plasma (B:P varying from 1.5 to 2.3 across species). This is likely due to enhanced  
364 partitioning through the acidic phospholipid bilayer of the cell membrane due to the weakly  
365 basic piperazine moiety. The higher partitioning into RBCs possibly contributes to a small  
366 degree to its potent *in vitro* and *in vivo* anti-*Plasmodium* activity by localizing the drug  
367 where the parasite resides.

368 As an indicator of hepatic metabolism, UCT943 was incubated across species with  
369 hepatocytes, liver microsomes, and liver S9 fraction (Table 2). The intrinsic clearance of  
370 UCT943 in both microsomes and hepatocytes was low in human, rat, and mouse ( $CL_{int} < 11.6$   
371  $\mu\text{L}/\text{min}/\text{mg}$  in microsomes and  $CL_{int} < 4 \mu\text{L}/\text{min}/10^6$  cells in hepatocytes), while it was  
372 moderate in dog ( $CL_{int} = 28.2 \mu\text{L}/\text{min}/\text{mg}$  in microsomes and  $CL_{int} = 9 \mu\text{L}/\text{min}/10^6$  cells in  
373 hepatocytes). Additionally, no significant metabolism ( $< 10\%$  degradation) was detected in  
374 human liver S9 fraction, showing that enzymes other than cytochrome P450s (CYPs) were  
375 not extensively involved in the metabolism of UCT943. No measurable inhibition was  
376 detected at  $20 \mu\text{M}$  against any of the CYP isoforms tested (CYP2D6, CYP2C9, CYP3A4/5),  
377 indicating that UCT943 has low potential for *in vivo* enzyme inhibition and that adverse  
378 drug-drug interactions through oxidative metabolism are likely to be minimal.  
379 Metabolite identification was performed *in vitro* using liver microsomes and hepatocytes, as  
380 well as *in vivo* by analyzing the collected blood samples from mouse PK experiments (Figure

5a). *In vitro*, liver microsomes and hepatocytes gave a complementary picture, both showing the major biotransformation pathway occurring on the piperazinylamide moiety (Figure 5b). UCT943 was mainly metabolized into an oxidation metabolite (P+16), which was further dehydrogenated into two metabolites P+14 (I&II) in non-human species. Further biotransformation on the piperazine ring gave metabolites P-26 (piperazine ring cleavage) and P+28. The formation of the carboxylic acid derivative by hydrolysis of the piperazinylamide moiety (P-68) was more easily detected in hepatocytes and *in vivo* in mice than in liver microsomes, presumably due to the higher concentration of the enzymes responsible for this particular biotransformation. The contribution of these metabolites to the activity of the parent UCT943 is currently under investigation. Notably, the P-68 metabolite, resulting from the hydrolysis of the carboxamide, showed high activity, albeit lower than that of the parent, with  $IC_{50}$ 's of 33 nM and 32 nM against *P. falciparum* NF54 and K1 strains respectively (6).

### 3.5 Pharmacokinetic studies

When administered intravenously, the blood clearance ( $CL_b$ ) of UCT943 was low in mice, rats, and dogs (Table 3), with a value of less than 20% of hepatic blood flow (23) to very low in monkeys with blood  $CL < 5\%$  hepatic blood flow, which is consistent with the high *in vitro* metabolic stability. Plasma volume of distribution was high in all species ( $V_{ss}$  7.1 - 13.1 L/kg), suggesting that the compound extensively distributes and accumulates in organ tissues. This would be expected for a basic compound due to partitioning into cell membranes by associating with acidic phospholipids (37). As a consequence of the low  $CL$  and high  $V_{ss}$ , half-lives were long, ranging from 6 h in mice to 29 h in monkeys. When dosed orally in mice and dogs, UCT943 was rapidly absorbed (time of maximum concentration  $T_{max} < 3$  h), while

404 absorption in rats and monkeys was slower with a maximum concentration ( $C_{\max}$ ) reached  
405 after 12 h and 7 h, respectively (Figure 6). Oral bioavailability was high across all species,  
406 ranging from 66% to 98%. The good oral bioavailability and the long  $t_{1/2}$  of UCT943 across  
407 species is encouraging toward achieving a single dose treatment and cure for malaria, which  
408 would boost patient compliance in resource-limited regions of the world, where the medical  
409 infrastructure is not sufficient. If these PK properties are confirmed in humans, UCT943  
410 could thus be a potential combination partner in a single exposure radical cure and  
411 prophylaxis (SERCaP) treatment as proposed by the Medicines for Malaria Venture (MMV)  
412 (34).

### 413 3.6 *In vivo* efficacy studies

414 When dosed at 10 mg/kg p.o., UCT943 reduced parasitemia by > 99.9% in the mouse *P.*  
415 *berghei* infection model and cured all mice with > 30 mean survival days (MSD). At 3 mg/kg  
416 p.o., no complete cure was achieved and MSD was 10 days (6), albeit parasitemia was  
417 reduced by 99%. The resulting 90% effective dose ( $ED_{90}$ ) was 1.0 mg/kg p.o. in the *P. berghei*  
418 infection model. In the *Pf*-infected NSG mouse model (Supplementary Material Figure S1),  
419 UCT943 was 2-fold more potent than MMV048 with a  $ED_{90}$  (90% effective dose) of 0.25  
420 mg/kg compared to 0.57 mg/kg (4). PK data showed that the exposure of UCT943 was dose-  
421 dependent (6). As PK/PD relationships in the humanized NSG mouse model have been found  
422 to be predictive of the induced blood-stage malaria (IBSM) model in human volunteers (38),  
423 we used the NSG mouse efficacy data for human dose prediction (see next section 3.7).

424 3.7 Prediction of human pharmacokinetics and efficacious single dose by PKPD modeling

425 3.7.1 Allometric scaling

426 The slope used to predict plasma CL by allometric scaling was close to 0.75 (0.73), while the  
427 slope used to predict plasma  $V_{ss}$  was close to 1 (0.90), as expected for metabolic processes  
428 and volumes, respectively (39) (Figure 7). The predicted human plasma  $V_{ss}$  was moderately  
429 large (6.3 L/kg) and the predicted human plasma CL was low (0.20 L/h/kg) as shown in Table  
430 4. When converted using the B:P ratio of 1.5, the predicted human blood clearance was 0.10  
431 L/h/kg, *i.e.* less than 10% of liver blood flow (23). The predicted  $t_{1/2}$  in humans was 27 h,  
432 which together with a long mean residence time of 32 h, suggests that the compound will  
433 be a long-duration antimalarial agent.

434 3.7.2 Estimation of minimum parasitocidal concentration (MPC) in blood in the *Pf*-infected

435 NSG mouse model

436 From the PK/PD model (Supplementary Material Figure S2 and S3), the compound specific  
437 PD parameters  $EC_{50}$  and  $K_{kill}$  were estimated to be 3.7 ng/mL and 0.060 /h respectively. The  
438 MPC in blood ( $MPC_b$ ), calculated using the  $EC_{50}$ , was 7.4 ng/mL in NSG mouse blood and 5.2  
439 ng/mL in human blood (Table 4), after correction for *Pf*-infected NSG mouse and human B:P  
440 partitioning data (2.8 and 1.5, respectively). The MPC in plasma ( $MPC_p$ ) used for human  
441 dose prediction was therefore 2.6 ng/mL. The *in vivo* parasite reduction ratio (PRR) of 48 h  
442 predicted by the PK/PD model (Log PRR = 1.25) correlated closely to the *in vitro* moderate  
443 killing profile (Log PRR = 2.5), confirming UCT943 as a slow acting antimalarial compound in  
444 this model.

## 445 3.7.3 Prediction of human pharmacokinetic parameters and efficacious dose

446 The human PK profiles modeled in Berkeley Madonna predicted a single human dose of 50-  
447 80 mg, based on dog and monkey data, respectively, in order to maintain the plasma  
448 concentrations above the predicted therapeutic level (that is, the plasma MPC<sub>p</sub> of 2.6  
449 ng/mL) for 8 days (*i.e.* four asexual parasite cycles) (Supplementary Material Figure S4 and  
450 S5). In this model, a single administration of the efficacious dose to maintain plasma  
451 concentrations above the MPC<sub>p</sub> for 8 days resulted in an area under the curve (AUC) of  
452 4213-8223 ng·h/mL, and a predicted C<sub>max</sub> of 234-358 ng/mL, based on monkey and dog,  
453 respectively. The low predicted dose is particularly encouraging, since it leaves a generous  
454 margin for potential dose increases, in case the predicted value was underestimated, or  
455 dose increase was deemed desirable to prevent the development of resistance or to ensure  
456 activity against other malaria species (including *P. vivax*, see section 3.1).

457 3.8 *In vitro* cytotoxicity, cardiotoxicity and genotoxicity

458 Cytotoxicity, assessed against four mammalian cell lines, was found to be low with a  
459 selectivity index (SI) greater than 2200 relative to the IC<sub>50</sub> in NF54 and greater than 170-fold  
460 against the highest IC<sub>50</sub> in *Pf* clinical isolates (Table 5). The SI is equivalent or greater than  
461 that of MMV048. Relative to the predicted upper unbound C<sub>max</sub> (0.13 μM) for the human  
462 efficacious plasma exposure, a 90-fold margin is thereby predicted and is sufficiently high to  
463 warrant progression into *in vivo* preclinical toxicology studies.

464 The safety margins over cardiotoxicity risk were largely improved compared to MMV048  
465 (see selectivity indexes SI in Table 5). The hERG IC<sub>50</sub> of 10 μM corresponds to an 80-fold  
466 margin relative to the predicted therapeutic unbound C<sub>max</sub> exposure for efficacy, which  
467 indicates a low risk of QT interval prolongation at therapeutic exposures. The margins to

468 potential safety issues associated with potential off-target activities at other ion channels  
469 ( $\text{Na}_v1.5$ ,  $\text{Ca}_v1.2$ , and  $\text{K}_v1.5$ ) are even higher (Table 5).  
470 Genotoxicity was evaluated using the Ames and mouse micronucleus tests, in which UCT943  
471 tested negative at the highest concentrations (Table 5), suggesting that the compound does  
472 not have the potential to result in back-mutation of a defective gene to recover its function  
473 (Ames test) (30), and does not have the ability to induce the formation of micronuclei during  
474 cell division as a consequence of genetic damage (micronucleus assay)(40).

### 475 3.9 *In vivo* G6PD-hemolysis

476 In the search for new antimalarial compounds, it is essential to develop drugs which do not  
477 pose a red blood cell hemolysis risk to patients with G6PD deficiency (34). When assessed  
478 for *in vivo* hemolytic toxicity in NOD-scid mice engrafted with A- G6PD-deficient human red  
479 blood cells (huRBCs), UCT943 showed comparable day 7 huRBC levels as those treated with  
480 the vehicle control, these levels being significantly higher when compared against the  
481 positive control primaquine (25 mg/kg/day). This indicates that UCT943 does not induce  
482 hemolytic toxicity at neither 1.5 nor 10 mg/kg/day dosing (Supplementary Material Figure  
483 S6), which is higher than the  $\text{ED}_{90}$  of 0.25 mg/kg in the *P. falciparum* NSG model of infection.  
484 Assessment of other markers of hemolysis, including spleen weight and mouse reticulocyte  
485 levels, also supports that UCT943 did not induce hemolytic toxicity (Supplementary Material  
486 Figures S7a and S7b).

## 487 4 CONCLUSION

488 UCT943 was optimized for antiparasmodial activity from a series of 2-aminopyrazines by  
489 structural modification of the clinical candidate MMV048, an inhibitor of an essential

490 *Plasmodium* enzyme, PI4K. Incorporation of a piperazinylamide group resulted in enhanced  
491 water solubility while maintaining high permeability, both parameters being key for a good  
492 developability profile and for achieving high drug exposure. This, combined with minimal *in*  
493 *vitro* metabolism in liver subcellular fractions and in hepatocytes, translated into low  
494 clearance, sustained exposure, and high bioavailability in preclinical species. UCT943 was  
495 potent against all stages of the *Plasmodium* parasite lifecycle, as well as against resistant *P.*  
496 *falciparum* and *P. vivax* clinical isolates. The 5-fold better *in vitro* antiplasmodial activity of  
497 UCT943 compared to MMV048 translated into excellent efficacy in the *P. berghei* mouse  
498 model and improved efficacy in the humanized *P. falciparum* mouse model. UCT943 was  
499 found to be a slow acting, long duration antimalarial compound similar to what is seen for  
500 quinoline antimalarials such as mefloquine. The predicted human single dose using monkey  
501 and dog pharmacokinetics was low, ranging from 50 to 80 mg, which offers considerable  
502 potential for the drug candidate. The high safety margins over cytotoxicity and cardiac  
503 toxicity highlighted herein are much larger than the predicted human therapeutic exposure,  
504 which is promising. Based on the data presented, UCT943 displays asexual blood stage,  
505 transmission-blocking, and liver stage activity and thus has the potential to form part of a  
506 single-exposure radical cure and prophylaxis (SERCAP) treatment of uncomplicated malaria.  
507 This breadth of activity offers considerable flexibility with respect to treatment options and  
508 TPPs that might be addressed and have contributed to the selection of UCT943 for  
509 preclinical development as a follow-on compound to MMV048.

510

511 **Acknowledgments:** This paper is dedicated to S.M. Solapur. The authors would like to  
512 acknowledge Nesia Barnes and Warren Olifant from H3D, University of Cape Town (South

513 Africa) for the ADME assays; Virgil Verhoog and Sumaya Salie from H3D, University of Cape  
514 Town (South Africa) for the *Pf* blood stage assays; Trevor Finch from the Division of  
515 Pharmacology, University of Cape Town (South Africa) for assistance with the animal work;  
516 Michael Delves, Andrea Ruecker and Robert E. Sinden from the Cell and Molecular Biology  
517 laboratory, Imperial College, London (United Kingdom) for the gamete formation assay;  
518 Anne-Marie Zeeman and Clemens H. M Kocken from the Biomedical Primate Research  
519 Centre, Rijswijk (The Netherlands) for the *Pc in vitro* prophylactic and radical cure assay;  
520 Rachaneeporn Jenwithisuk from the Faculty of Tropical Medicine, Mahidol University,  
521 Bangkok (Thailand) for the *Pv in vitro* prophylactic and radical cure assay; John Burke from  
522 the University of Victoria, British Columbia (Canada) for the *Pv*PI4K assay.

523

524 **Funding:** We acknowledge the Medicines for Malaria Venture (project MMV09/0002),  
525 Technology Innovation Agency (TIA) and the Strategic Health Innovation Partnerships (SHIP)  
526 unit of the South African Medical Research Council (SAMRC) for financial support of this  
527 research. K.C. acknowledges support from the University of Cape Town, SAMRC and South  
528 African Research Chairs Initiative of the Department of Science and Technology  
529 administered through the National Research Foundation. L.B. and T.C also acknowledge  
530 support of SHIP.



531 Tables

532 **Table 1: Physico-chemical properties of UCT943 compared to MMV048**

Property (SD)		UCT943	MMV048
MW (g/mol)		427.4	393.4
LogD	pH 7.4	-0.27 (0.01)	2.6 (0.03)
pKa	measured	7.45 (0.05)	4.0 (0.07)
Thermodynamic solubility (µg/mL)*	pH 2.0	3000	740
	pH 4.0	49	-
	pH 6.0	110	4.2 (pH 6.5)
	pH 8.0	31	4.0 (pH 7.4)
	pH 10.0	8.3	-
	SGF (pH 1.8)	5900	-
	FaSSIF (pH 6.5)	1500	14.4
	FeSSIF (pH 5.0)	1900	28.3 (pH 5.8)

533 SGF: Simulated Gastric Fluid; FaSSIF: Fasted State Simulated Intestinal Fluid; FeSSIF: Fed

534 State Simulated Intestinal Fluid

535 \* single determination

536 **Table 2: In vitro metabolism, permeability, protein binding, blood:plasma ratio and**  
 537 **plasma stability data for UCT943**

<i>Parameter h/d/r/m (SD)</i>	
Microsomal CL <sub>int</sub> (μL/min/mg)	<11.6 (0.1) / 28.2 (0.5) / <11.6 (0.2) / <11.6 (0.7)
Hepatocyte CL <sub>int</sub> (μL/min/10 <sup>6</sup> cells)*	<2 / 9 / 4 / <4
Hepatocyte predicted E <sub>H</sub> *	<0.2 / 0.65 / 0.23 / <0.2
Caco-2 P <sub>app</sub> B>A / P <sub>app</sub> A>B (10 <sup>-6</sup> cm/s)	25 (5) / 28 (2)
f <sub>u</sub> microsomes	0.15 (0.01) / 0.50 (0.04) / 0.45 (0.05) / 0.47 (0.04)
f <sub>u</sub> plasma	0.17 (0.009) / 0.10 (0.007) / 0.15 (0.009) / 0.10 (0.02)
Blood:Plasma ratio	1.5 (0.1) / 2.3 (0.1) / 2.1 (0.2) / 1.9 (0.2)
Plasma stability (% after 240 min)*	97 / 95 / 97 / 102

538 \* single determination

539 **Table 3: In vivo pharmacokinetic parameters for UCT943 across mouse, rat, dog, and**  
 540 **monkey species calculated from non-compartmental analysis (SD are given in brackets)**

Species	Mouse	Mouse	Rat	Rat	Dog	Dog	Monkey	Monkey
Dose (mg/kg)	5 (IV)	20 (PO)	5 (IV)	20 (PO)	2 (IV)	10 (PO)	2 (IV)	10 (PO)
$t_{1/2}$ (h)	6.4 (0.7)	5.7 (0)	7.4 (0.6)	5.3 (0.3)	13.0	16.1	28.6	34.6
Plasma $V_{ss}$ (L/kg)	13.1* (1.1)	-	11.5*(2.1)	-	7.1 (0.9)	-	8.7 (1.0)	-
Blood $CL_b$ (mL/min/kg)	12.6 (2.4)	-	9.5 (1.6)	-	3.3* (0.6)	-	2.0 *(0.3)	-
Plasma $CL_p$ (mL/min/kg)	24.0* (4.6)	-	20.0*(3.4)	-	7.5 (1.2)	-	3.9 (0.6)	-
Plasma $AUC_{0-\infty p}$ (min· $\mu$ M)	497* (8.5)	1310*(202)	725*(109)	2843*(480)	634 (89)	2335 (754)	1192 (164)	4745 (761)
Plasma $C_{max}$ ( $\mu$ M)	1.2* (0.2)	1.7* (0.3)	2.4*(0.2)	2.1*(0.7)	1.0 (0.1)	2.3 (0.4)	1.5 (0.03)	2.1 (0.4)
$T_{max}$ (h)	-	4.0 (3.6)	-	12.0	-	2.3 (1.5)	-	7.0 (1.7)
F (%)	-	66 (10)	-	98 (4.9)	-	74 (23.7)	-	80 (12.8)

541 \*blood values were scaled to plasma values using B:P ratios of 1.9/2.1/2.3/2.0 for mice, rats,

542 dogs, and monkeys, respectively

543 <sub>b</sub> blood; <sub>p</sub> plasma

544 **Table 4: Predicted human PK parameters for UCT943 from modeling**

Parameter	UCT943
Plasma $V_{ss}$ (L/kg)	6.3
Plasma $CL_p$ (L/h/kg)	0.20
MRT (h)	32
Plasma $MPC_p$ (ng/mL); blood $MPC_b$ (ng/mL);	2.6; 5.2
$k_a$ (/h)	0.25
F (%)	80
Single dose (mg)*	50-80
$t_{1/2}$ (h)	27
Plasma $AUC_p$ (ng·h/mL)	4213-8223
Plasma $C_{max,p}$ (ng/mL)	234-358

545 MPC: Minimum Parasitocidal Concentration

546 \*Predicted single dose to achieve  $\geq 8$  days above MPC

547 <sub>b</sub> blood; <sub>p</sub> plasma

548 **Table 5: Cytotoxicity, cardiotoxicity and genotoxicity data for UCT943 and MMV048**

		MMV048	UCT943	
	Cell line / Ion channel	CC <sub>50</sub> $\mu$ M (SI)	CC <sub>50</sub> $\mu$ M (SI)	Lowest SI
Cytotoxicity	CHO	-	17 (3148x)	298
	Vero	-	113 (20926x)	1982
	HepG2	>10 (357x)	13 (2407x)	225
	L6	251 (8964x)	12 (2222x)	211
Cardiotoxicity	hERG (K <sub>v</sub> 11.1)	>11 (393x)	10 [6.4-15.9] (1870x)	177
	Na <sub>v</sub> 1.5	100 (3571x)	>33 (>6111x)	>579
	Ca <sub>v</sub> 1.2	16 (571x)	>33 (>6111x)	>579
	K <sub>v</sub> 1.5	-	>33 (>6111x)	>579
Genotoxicity	Ames assay	Negative	Negative	-
	Micronucleus test	Negative	Negative	-

549 CC<sub>50</sub>: 50% cytotoxic concentration

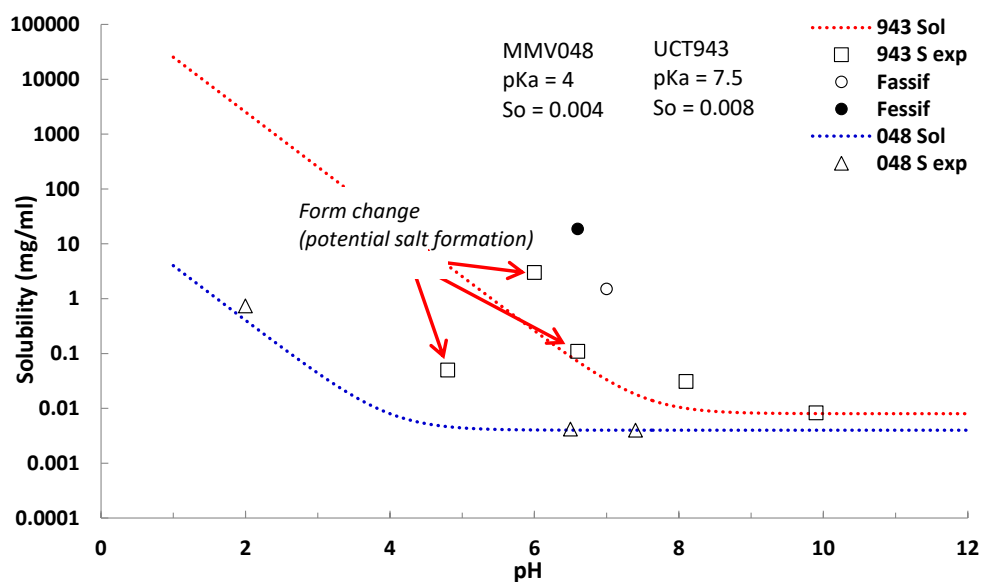
550 IC<sub>50</sub>: 50% inhibitory concentration

551 SI: selectivity index; SI = CC<sub>50</sub> / IC<sub>50</sub> NF54 ;

552 Lowest SI; lowest selectivity index against clinical isolates; lowest SI = CC<sub>50</sub> / max IC<sub>50</sub> Pf

553 clinical isolate

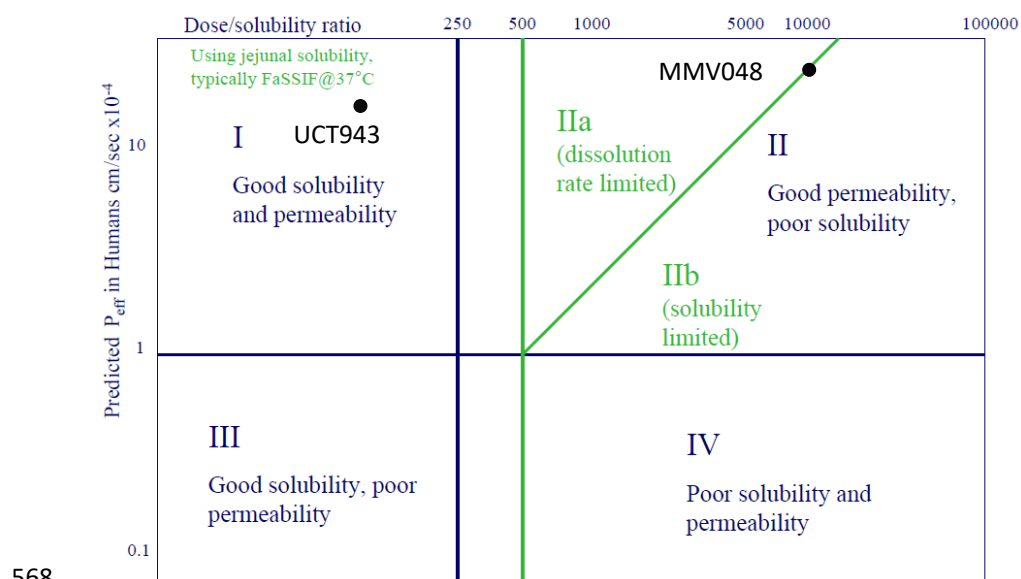




563

564 **Figure 3: Comparison of pH solubility profiles of MMV048 (dotted blue line) and UCT943**  
 565 **(dotted red line) calculated and measured values for MMV048 (triangle dots), and UCT943**  
 566 **(square dots)**

567 FaSSiF: Fasted State Simulated Intestinal Fluid; FeSSiF: Fed State Simulated Intestinal Fluid

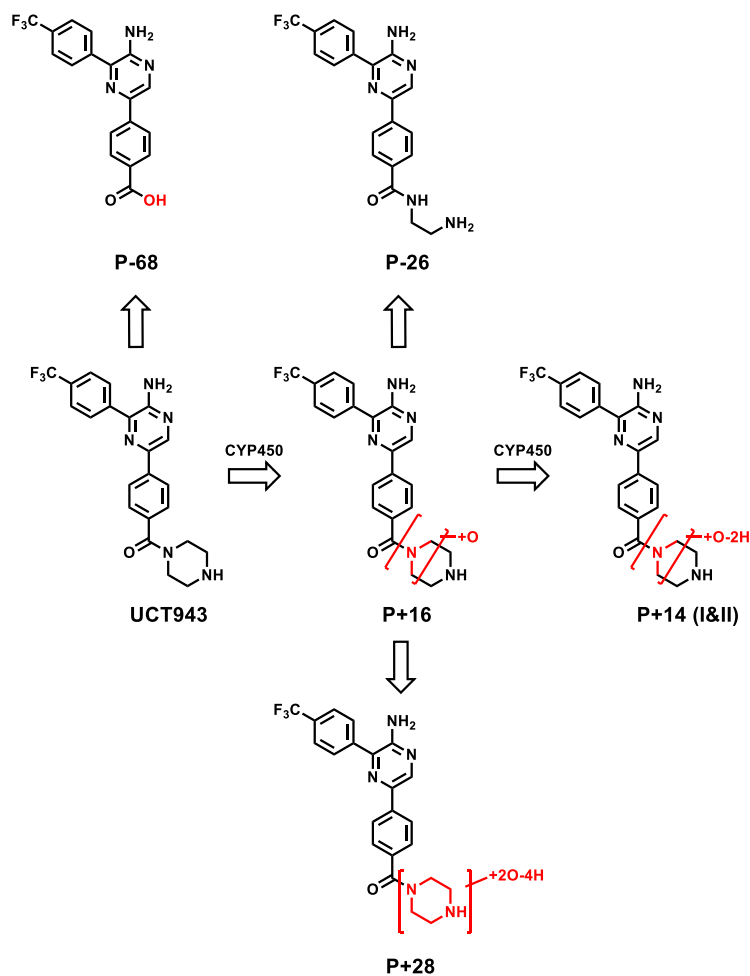


568

569 **Figure 4: Ranking of UCT943 and MMV048 in the Developability Classification System**

570 **(DCS) (36).**

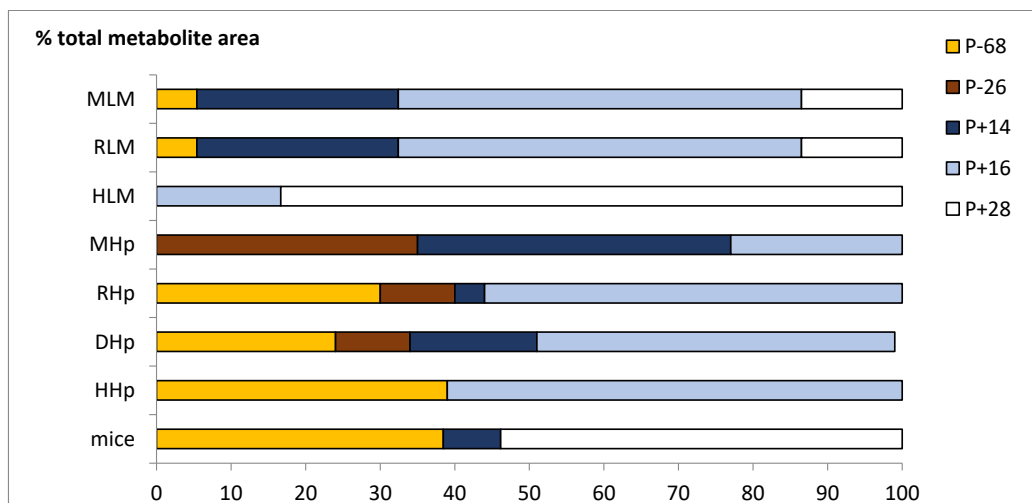




571

572 **Figure 5a: Proposed metabolic pathway of UCT943 in microsomes (mouse, rat, human),**

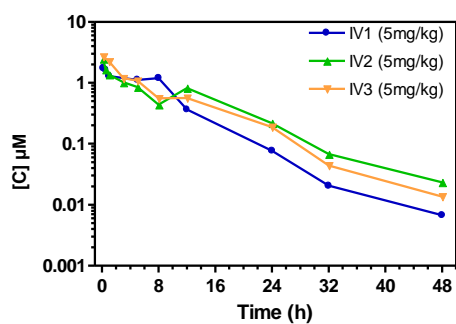
573 **hepatocytes and in vivo in mice**



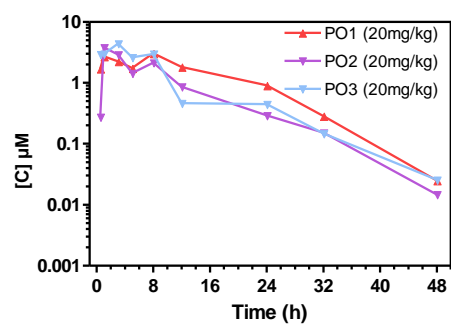
574

575 **Figure 5b: Metabolite profiles of UCT943 in liver microsomes, hepatocytes, and in mice**

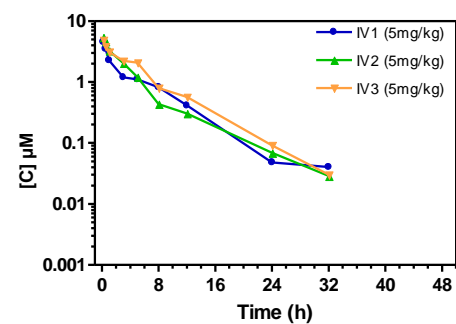
576 LM: liver microsomes; Hp: hepatocytes; H: human; R: rat; M: mice; D: dog



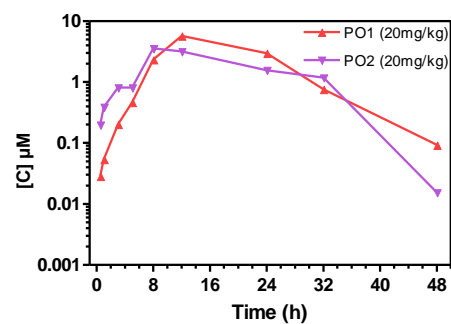
(a)



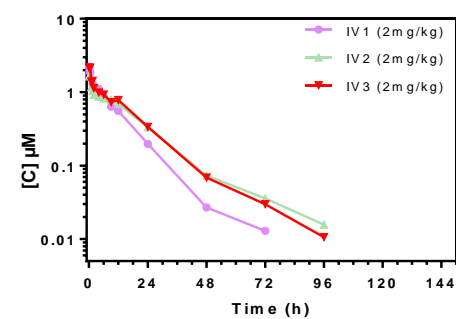
(b)



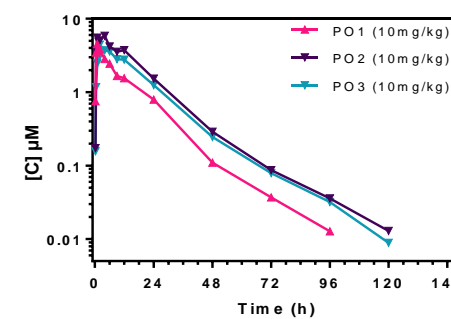
(c)



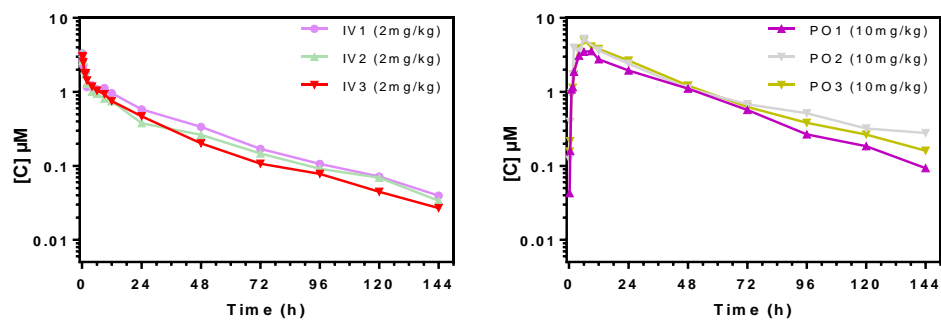
(d)



(e)



(f)



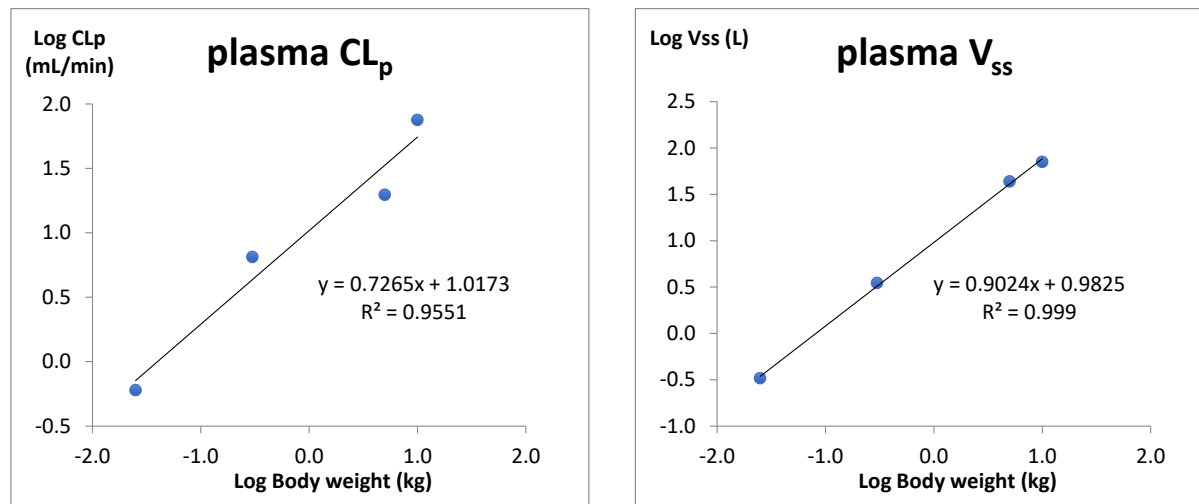
583  
584

(g)

(h)

585 **Figure 6: Whole blood concentration vs time profiles following IV (left) and oral (right)**  
586 **administration of UCT943 to (a, b) non-fasted male Balb/C mice; (c, d) fasted male**  
587 **Sprague Dawley rats; (e, f) fasted male beagle dogs; (g, h) fasted female Cynomolgus**  
588 **monkeys**

589



592

(a)

(b)

593 **Figure 7: Allometric plot for UCT943 (a) plasma clearance and (b) plasma volume of**

594 **distribution**

## 595 References

1. WHO (World Health Organisation). 2017. World malaria report 2017, 160p.
2. Takala-Harrison S, Laufer MK. 2015. Antimalarial drug resistance in Africa: key lessons for the future. *Ann N Y Acad Sci* 1342:62–67.
3. Mbengue A, Bhattacharjee S, Pandharkar T, Liu H, Estiu G, Stahelin R V., Njimoh DL, Ryan Y, Chotivanich K, Nguon C, Ghorbal M, Lopez-Rubio JJ, Pfrender M, Emrich S, Mohandas N, Dondorp AM, Wiest O, Haldar K. 2015. A molecular mechanism of artemisinin resistance in *Plasmodium falciparum* malaria. *Nature* 520:683–687.
4. Paquet T, Le Manach C, González Cabrera D, Younis Y, Henrich PP, Abraham TS, Lee MCS, Basak R, Ghidelli-Disse S, Lafuente-Monasterio MJ, Bantscheff M, Ruecker A, Blagborough AM, Zakutansky SE, Zeeman A-M, White KL, Shackleford DM, Mannila J, Morizzi J, Scheurer C, Angulo-Barturen I, Santos-Martínez M, Ferrer S, Sanz LM, Gamo FJ, Reader J, Botha MJ, Dechering KJ, Sauerwein RW, Tungtaeng A, Vanachayangkul P, Lim CS, Burrows JN, Witty MJ, Marsh KC, Bodenreider C, Rochford R, Solapure SM, Jiménez-Díaz MB, Wittlin S, Charman SA, Donini C, Campo B, Birkholtz L-M, Hanson KK, Drewes G, Kocken CHM, Delves MJ, Leroy D, Fidock DA, Waterson D, Street LJ, Chibale K. 2017. Antimalarial efficacy of MMV390048, an inhibitor of *Plasmodium* phosphatidylinositol 4-kinase. *Sci Transl Med* 9:eaad9735.
5. McNamara CW, Lee MCS, Lim CS, Lim SH, Roland J, Nagle A, Simon O, Yeung BKS, Chatterjee AK, McCormack SL, Manary MJ, Zeeman A-M, Dechering KJ, Kumar TRS, Henrich PP, Gagaring K, Ibanez M, Kato N, Kuhen KL, Fischli C, Rottmann M, Plouffe DM, Bursulaya B, Meister S, Rameh L, Trappe J, Haasen D, Timmerman M, Sauerwein RW, Suwanarusk R, Russell B, Renia L, Nosten F, Tully DC, Kocken CHM, Glynn RJ, Bodenreider C, Fidock DA, Diagana TT, Winzeler EA. 2013. Targeting *Plasmodium*

- PI(4)K to eliminate malaria. *Nature* 504:248–253.
6. Le Manach C, Nchinda AT, Paquet T, Gonzalez Cabrera D, Younis Y, Han Z, Bashyam S, Zabiulla M, Taylor D, Lawrence N, White KL, Charman SA, Waterson D, Witty MJ, Wittlin S, Botha ME, Nondaba SH, Reader J, Birkholtz L-M, Jimenez-Diaz M-B, Santos Martinez M, Ferrer S, Angulo-Barturen I, Meister S, Antonova-Koch Y, Winzeler EA, Street LJ, Chibale K. 2016. Identification of a potential antimalarial drug candidate from a series of 2-aminopyrazines by optimization of aqueous solubility and potency across the parasite life cycle. *J Med Chem* 59:9890–9905.
  7. Desjardins RE, Canfield CJ, Haynes JD, Chulay JD. 1979. Quantitative assessment of antimalarial activity *in vitro* by a semiautomated dilution technique. *Antimicrob Agents Chemother* 16:710–718.
  8. Matile H, Pink JRL. 1990. *Plasmodium falciparum* malaria parasite cultures and their use in immunology, p. 221–234. In Lefkovits, I. & Pernis, B., E (ed.), *Immunological Methods*. Academic Press, San Diego, CA, USA.
  9. Phillips MA, White KL, Kokkonda S, Deng X, White J, El Mazouni F, Marsh K, Tomchick DR, Manjulanagara K, Rudra KR, Wirjanata G, Noviyanti R, Price RN, Marfurt J, Shackleford DM, Chiu FCK, Campbell M, Jimenez-Diaz MB, Bazaga SF, Angulo-Barturen I, Martinez MS, Lafuente-Monasterio M, Kaminsky W, Silue K, Zeeman A-M, Kocken C, Leroy D, Blasco B, Rossignol E, Rueckle T, Matthews D, Burrows JN, Waterson D, Palmer MJ, Rathod PK, Charman SA. 2016. A triazolopyrimidine-based dihydroorotate dehydrogenase inhibitor with improved drug-like properties for treatment and prevention of malaria. *ACS Infect Dis* 2:945–957.
  10. Silvie O, Rubinstein E, Franetich J-F, Prenant M, Belnoue E, Rénia L, Hannoun L, Eling W, Levy S, Boucheix C, Mazier D. 2003. Hepatocyte CD81 is required for *Plasmodium*

- falciparum* and *Plasmodium yoelii* sporozoite infectivity. Nat Med 9:93–96.
11. Yalaoui S, Zougbedé S, Charrin S, Silvie O, Arduise C, Farhati K, Boucheix C, Mazier D, Rubinstein E, Froissard P. 2008. Hepatocyte permissiveness to *Plasmodium* infection is conveyed by a short and structurally conserved region of the CD81 large extracellular domain. PLoS Pathog 4:e1000010.
  12. Zeeman AM, Van Amsterdam SM, McNamara CW, Voorberg-van Der Wel A, Klooster EJ, Van Den Berg A, Remarque EJ, Plouffe DM, Van Gemert GJ, Luty A, Sauerwein R, Gagaring K, Borboa R, Chen Z, Kuhen K, Glynn RJ, Chatterjee AK, Nagle A, Roland J, Winzeler EA, Leroy D, Campo B, Diagana TT, Yeung BKS, Thomas AW, Kocken CHM. 2014. KAI407, a potent non-8-aminoquinoline compound that kills *Plasmodium cynomolgi* early dormant liver stage parasites in vitro. Antimicrob Agents Chemother 58:1586–1595.
  13. Sattabongkot J, Yimamnuaychoke N, Leelaudomlapi S, Rasameesoraj M, Jenwithisuk R, Coleman RE, Udomsangpetch R, Cui L, Brewer TG. 2006. Establishment of a human hepatocyte line that supports *in vitro* development of the exo-erythrocytic stages of the malaria parasites *Plasmodium falciparum* and *P. vivax*. Am J Trop Med Hyg 74:708–715.
  14. Reader J, Botha M, Theron A, Lauterbach SB, Rossouw C, Engelbrecht D, Wepener M, Smit A, Leroy D, Mancama D, Coetzer TL, Birkholtz L-M. 2015. Nowhere to hide: interrogating different metabolic parameters of *Plasmodium falciparum* gametocytes in a transmission blocking drug discovery pipeline towards malaria elimination. Malar J 14:1–17.
  15. Ruecker A, Mathias DK, Straschil U, Churcher TS, Dinglasan RR, Leroy D, Sinden RE, Delves MJ. 2014. A male and female gametocyte functional viability assay to identify



- biologically relevant malaria transmission-blocking drugs. *Antimicrob Agents Chemother* 58:7292–7304.
16. Baragaña B, Hallyburton I, Lee MCS, Norcross NR, Grimaldi R, Otto TD, Proto WR, Blagborough AM, Meister S, Wirjanata G, Ruecker A, Upton LM, Abraham TS, Almeida MJ, Pradhan A, Porzelle A, Martínez MS, Bolscher JM, Woodland A, Luksch T, Norval S, Zuccotto F, Thomas J, Simeons F, Stojanovski L, Osuna-Cabello M, Brock PM, Churcher TS, Sala KA, Zakutansky SE, Jiménez-Díaz MB, Sanz LM, Riley J, Basak R, Campbell M, Avery VM, Sauerwein RW, Dechering KJ, Noviyanti R, Campo B, Frearson JA, Angulo-Barturen I, Ferrer-Bazaga S, Gamo FJ, Wyatt PG, Leroy D, Siegl P, Delves MJ, Kyle DE, Wittlin S, Marfurt J, Price RN, Sinden RE, Winzeler EA, Charman SA, Bebrevska L, Gray DW, Campbell S, Fairlamb AH, Willis PA, Rayner JC, Fidock DA, Read KD, Gilbert IH. 2015. A novel multiple-stage antimalarial agent that inhibits protein synthesis. *Nature* 522:315–320.
17. Gibhard L, Pravin K, Abay E, Wilhelm A, Swart K, Lawrence N, Khoury R, van der Westhuizen J, Smith P, Lubbe Wiesner. 2016. *In Vitro* and *in vivo* pharmacokinetics of aminoalkylated diarylpropanes NP085 and NP102. *Antimicrob Agents Chemother* 60:3065–3069.
18. Phillips MA, Lotharius J, Marsh K, White J, Dayan A, White KL, Njoroge JW, Mazouni F El, Lao Y, Kokkonda S, Tomchick DR, Deng X, Laird T, Bhatia SN, March S, Ng CL, Fidock DA, Wittlin S, Lafuente-Monasterio M, Gamo Benito JF, Sanz Alonso LM, Santos Martinez M, Jimenez-Diaz, Maria Belen Ferrer Bazaga S, Angulo-Barturen I, Haselden JN, Louttit J, Cui Y, Sridhar A, Zeeman A-M, Kocken C, Sauerwein R, Dechering K, Avery VM, Duffy S, Delves M, Sinden R, Ruecker A, Wickham, Kristina S. Rochford R, Gahagen J, Iyer L, Riccio E, Mirsalis J, Bathhurst I, Rueckle T, Ding X,

- Campo B, Leroy D, Rogers MJ, Rathod PK, Burrows JN, Charman SA. 2015. A long-duration dihydroorotate dehydrogenase inhibitor (DSM265) for prevention and treatment of malaria. *Sci Transl Med* 7:296ra111.
19. Ring BJ, Chien JY, Adkison KK, Jones HM, Rowland M, Jones R Do, Yates JWT, Ku MS, Gibson CR, He H, Vuppugalla R, Marathe P, Fischer V, Dutta S, Sinha VK, Björnsson T, Lavé T, Poulin P. 2011. PhRMA CPCDC initiative on predictive models of human pharmacokinetics, part 3: Comparative assessment of prediction methods of human clearance. *J Pharm Sci* 100:4090–4110.
20. Coteron JM, Marco M, Esquivias J, Deng X, White KL, White J, Koltun M, El Mazouni F, Kokkonda S, Katneni K, Bhamidipati R, Shackleford DM, Angulo-Barturen I, Ferrer SB, Jiménez-Díaz MB, Gamo F-J, Goldsmith EJ, Charman WN, Bathurst I, Floyd D, Matthews D, Burrows JN, Rathod PK, Charman SA, Phillips MA. 2011. Structure-guided lead optimization of triazolopyrimidine-ring substituents identifies potent *Plasmodium falciparum* dihydroorotate dehydrogenase inhibitors with clinical candidate potential. *J Med Chem* 54:5540–5561.
21. Walsky RL, Obach RS. 2004. Validated assays for human cytochrome P450 activities. *Drug Metab Dispos* 32:647–60.
22. Le Manach C, Paquet T, Brunschwig C, Njoroge M, Han Z, Gonzalez Cabrera D, Bashyam S, Dhinakaran R, Taylor D, Reader J, Botha M, Churchyard A, Lauterbach S, Coetzer T, Birkholtz L-M, Meister S, Winzeler EA, Waterson D, Witty MJ, Wittlin S, Jimenez-Diaz M-B, Santos Martinez M, Ferrer S, Angulo-Barturen I, Street LJ, Chibale K. 2015. A novel pyrazolopyridine with in vivo activity in *Plasmodium berghei*- and *Plasmodium falciparum*-infected mouse models from structure-activity relationship studies around the core of recently identified antimalarial imidazopyridazines. *J Med*

- Chem 58:8713–8722.
23. Davies B, Morris T. 1993. Physiological parameters in laboratory animals and humans. *Pharm Res* 10:1093–1095.
24. Jiménez-Díaz MB, Mulet T, Viera S, Gómez V, Garuti H, Ibáñez J, Alvarez-Doval A, Shultz LD, Martínez A, Gargallo-Viola D, Angulo-Barturen I. 2009. Improved murine model of malaria using *Plasmodium falciparum* competent strains and non-myelodepleted NOD-*scid* *IL2Rγ<sup>null</sup>* mice engrafted with human erythrocytes. *Antimicrob Agents Chemother* 53:4533–4536.
25. Boxenbaum H. 1982. Interspecies scaling, allometry, physiological time, and the ground plan of pharmacokinetics. *J Pharmacokinet Biopharm* 10:201–227.
26. Wajima T, Yano Y, Fukumura K, Oguma T. 2004. Prediction of human pharmacokinetic profile in animal scale up based on normalizing time course profiles. *J Pharm Sci* 93:1890–1900.
27. Mosmann T. 1983. Rapid colorimetric assay for cellular growth and survival: Application to proliferation and cytotoxicity assays. *J Immunol Methods* 65:55–63.
28. Rubinstein L V., Shoemaker RH, Paull KD, Simon RM, Tosini S, Skehan P, Scudiero DA, Monks A, Boyd MR. 1990. Comparison of *in vitro* anticancer-drug-screening data generated with a tetrazolium assay against a diverse panel of human tumor cell lines. *J Natl Cancer Inst* 82:1113–1118.
29. Schroeder K, Neagle B, Trezise DJ, Worley J. 2003. IonWorks (TM) HT: A new high-throughput electrophysiology measurement platform. *J Biomol Screen* 8:50–64.
30. Mortelmans K, Zeiger E. 2000. The Ames *Salmonella*/microsome mutagenicity assay. *Mutat Res* 455:29–60.
31. Mortelmans K, Riccio ES. 2000. The bacterial tryptophan reverse mutation assay with

- Escherichia coli* WP2. Mutat Res - Fundam Mol Mech Mutagen 455:61–69.
32. Rochford R, Ohrt C, Baresel PC, Campo B, Sampath A, Magill AJ, Tekwani BL, Walker LA. 2013. Humanized mouse model of glucose 6-phosphate dehydrogenase deficiency for *in vivo* assessment of hemolytic toxicity. Proc Natl Acad Sci U S A 110:17486–17491.
33. LaMarche MJ, Borawski J, Bose A, Capacci-Daniel C, Colvin R, Dennehy M, Ding J, Dobler M, Drumm J, Gaither LA, Gao J, Jiang X, Lin K, McKeever U, Puyang X, Raman P, Thohan S, Tommasi R, Wagner K, Xiong X, Zabawa T, Zhu S, Wiedmann B. 2012. Anti-hepatitis C virus activity and toxicity of type III phosphatidylinositol-4-kinase beta inhibitors. Antimicrob Agents Chemother 56:5149–5156.
34. Burrows JN, Duparc S, Gutteridge WE, van Huijsduijnen R, Kaszubska W, Macintyre F, Mazzuri S, Möhrle JJ, Wells TNC. 2017. New developments in anti-malarial target candidate and product profiles. Malar J 16:26.
35. Van der Watt M, Reader J, Churchyard A, Nondaba SH, Lauterbach SB, Niemand J, Abayomi S, Van Biljon RA, Connacher JJ, Van Wyk RDJ, Le Manach C, Paquet T, Gonzalez Cabrera D, Brunschwig C, Theron A, Lozano-Arias S, Rodrigues JFI, Herreros E, Leroy D, Duffy J, Street LJ, Chibale K, Mancama D, Coetzer TL, Birkholtz L-M. 2018. Potent *Plasmodium falciparum* gametocytocidal compounds identified by exploring the kinase inhibitor chemical space for dual active antimalarials. J Antimicrob Chemother in press.
36. Butler JM, Dressman JB. 2010. The Developability Classification System : application of biopharmaceutics concepts to formulation development. J Pharm Sci 99:4940–4954.
37. Smith DA, Di L, Kerns EH. 2010. The effect of plasma protein binding on *in vivo*

- efficacy: misconceptions in drug discovery. *Nat Rev Drug Discov* 9:929–939.
38. McCarthy JS, Marquart L, Sekuloski S, Trenholme K, Elliott S, Griffin P, Rockett R, O'Rourke P, Sloots T, Angulo-Barturen I, Ferrer S, Jiménez-Díaz MB, Santos Martinez M, Hooft van Huijsduijnen R, Duparc S, Leroy D, Wells TNC, Baker M, Möhrle JJ. 2016. Linking murine and human *Plasmodium falciparum* challenge models in a translational path for antimalarial drug development. *Antimicrob Agents Chemother* 60:3669–3675.
39. Anderson BJ, Holford NHG. 2008. Mechanism-based concepts of size and maturity in pharmacokinetics. *Annu Rev Pharmacol Toxicol* 48:303–332.
40. Corvi R, Albertini S, Hartung T, Hoffmann S, Maurici D, Pfuhler S, Van Benthem J, Vanparys P. 2008. ECVAM retrospective validation of *in vitro* micronucleus test (MNT). *Mutagenesis* 23:271–283.